Quaternary Science Reviews 215 (2019) 160–172

Contents lists available at ScienceDirect

Quaternary Science Reviews

journal homepage: www.elsevier.com/locate/quascirev

Holocene temperature history of northwest Greenland – With new ice cap constraints and chironomid assemblages from Deltasø

Y. Axford [a, *], G.E. Lasher [a], M.A. Kelly [b], E.C. Osterberg [b], J. Landis [b], G.C. Schellinger [a], A. Pfeiffer [a], E. Thompson [b], D.R. Francis [c]

[a] Department of Earth and Planetary Sciences, Northwestern University, 2145 Sheridan Road, Evanston, IL 60208, USA
[b] Department of Earth Sciences, Dartmouth College, Hanover, NH, USA
[c] Department of Geosciences, University of Massachusetts, Amherst, MA, USA

ARTICLE INFO

Article history:
Received 14 March 2019
Received in revised form
11 May 2019
Accepted 13 May 2019
Available online 25 May 2019

Keywords:
Greenland
Arctic
Holocene thermal maximum
Lake sediments
Chironomids
Glaciers
Paleotemperatures

ABSTRACT

Arctic temperature shifts drive changes in carbon cycling, sea ice extent and Greenland Ice Sheet mass balance, all of which have global ramifications. Paleoclimate data from past warm periods provide a unique means for assessing the sensitivity of these systems to warming climate, but the magnitude and timing of past temperature changes in many parts of the Arctic are poorly known. Here we assess orbital-scale Holocene temperature change in northwest Greenland near the margin of the ice sheet using subfossil insect assemblages from lake Deltasø. Based upon sedimentation history in this currently proglacial lake, we also place constraints on Holocene extents of the adjacent North Ice Cap, a large independent ice cap. Reconstructed summer temperatures were warmer than present at the onset of lacustrine sedimentation following regional deglaciation by the Greenland Ice Sheet, sometime between 10.8 and 10.1 ka BP. Deltasø experienced the warmest summer temperatures of the Holocene between ~10 and 6.2 ka BP, followed by progressive cooling that continued through the late Holocene as summer insolation declined, culminating in the lowest temperatures during the pre-industrial last millennium. Deltasø chironomids indicate peak early Holocene summer temperatures at least 2.5–3 °C warmer than modern and at least 3.5–4 °C warmer than the pre-industrial last millennium. We infer based upon lake sediment organic and biogenic content that in response to declining temperatures, North Ice Cap reached its present-day size ~1850 AD, having been smaller than present through most of the preceding Holocene. Our synthesis of paleoclimate evidence from northwest Greenland, Ellesmere Island and northern Baffin Bay supports the timing of temperature trends inferred at Deltasø, and suggests that quantitative temperature reconstructions from Deltasø may represent a minimum bound on regional early Holocene warming. Collectively, records from the region indicate >4 °C summer cooling through the Holocene. Intense early Holocene warmth around northwest Greenland argues against delayed onset of warmer-than-present conditions due to the influence of the nearby waning Laurentide Ice Sheet, and has implications for understanding the Greenland Ice Sheet's sensitivity to climate change.

1. Introduction

Much of the Arctic experienced peak Holocene warmth during a period of enhanced summer insolation in the early to middle Holocene (Kaufman, 2004). Such past warm periods offer insights into the consequences of future arctic warming. Around Greenland, for example, flora and fauna migrated northward and sea ice was at times less extensive off the Arctic Ocean coast (Bennike, 2004; Dyke et al., 1996; Funder, 1978; Funder et al., 2011a; Funder and Weidick, 1991). Large sectors of the Greenland Ice Sheet margin and many independent ice caps and glaciers retreated to positions smaller than today (Funder et al., 2011b; Larsen et al., 2015, 2017; Levy et al., 2014; Weidick and Bennike, 2007; Young and Briner, 2015). The extent of retreat is poorly known, however, as is the magnitude of temperature change that drove retreat.

Warm-season temperatures near the ice sheet margins drive ice sheet melt, and as such are essential to understanding ice sheet sensitivity to climate change. Yet there are few continuous,

* Corresponding author.
E-mail address: axford@northwestern.edu (Y. Axford).

https://doi.org/10.1016/j.quascirev.2019.05.011
0277-3791/

quantitative reconstructions of past summer temperatures around Greenland's margins. A recent reinterpretation of oxygen isotope measurements from Agassiz ice cap on Ellesmere Island (Fig. 1) demonstrated both the large uncertainty in Holocene temperature reconstructions from this region and their importance to understanding ice sheet behavior and thus sea level change (Lecavalier et al., 2017). We lack strong constraints on Holocene temperatures in Greenland to compare with observations of past ice sheet changes and to employ as forcings in tests of ice sheet models (Lecavalier et al., 2014; Simpson et al., 2009; Sinclair et al., 2016; Young and Briner, 2015). A recent study of the Last Interglacial and early Holocene suggests that summer temperatures over northern Greenland may have been generally underestimated in model and synthesis studies, with important consequences for ice sheet behavior (McFarlin et al., 2018).

Here we present new results from the small lake Deltasø in northwest Greenland, and summarize regional evidence for Holocene temperature trends, including results from several studies published in the past three years. We reconstruct July air temperatures based upon insect (Diptera: Chironomidae) assemblages preserved in Deltasø's sediments. Chironomid species distributions are temperature-sensitive (Brooks et al., 2012; Eggermont and Heiri, 2012; Walker et al., 1991), and the remains of their aquatic larvae are abundant and well preserved in the sediments of many arctic lakes. Chironomids have been used for quantitative paleotemperature reconstructions at only a few sites in Greenland (Axford et al., 2013, 2017; McFarlin et al., 2018; Wooller et al., 2004). However, this proxy has long been used as a qualitative paleoenvironmental indicator (Brodersen and Bennike, 2003; Wagner et al., 2005), and has been widely employed for quantitative paleotemperature reconstructions elsewhere in the Arctic and subarctic (e.g., see multi-proxy reviews by Briner et al. (2016); Kaufman et al. (2016)). We argue that very high-latitude lakes like Deltasø are especially well-suited to developing Holocene paleotemperature reconstructions from chironomid assemblages, given the reduced effects of potentially confounding Holocene changes in vegetation and soil development at these sites (Axford et al., 2017).

In addition, by capturing glacial sediments from a stream draining the Knud Rasmussen outlet glacier of North Ice Cap, Deltasø sediments register past ice cap extent. Independent glaciers and ice caps respond sensitively to local climate and provide a proxy for ablation season temperature near the Greenland Ice Sheet margin (Levy et al., 2014; Lowell et al., 2013), but the history of independent ice caps in northwest Greenland is poorly known. Based upon subfossil plants recovered from a shear plane in North Ice Cap that dated to 5.4 ka BP (ka BP = thousands of years before 1950 AD), Goldthwait (1960) hypothesized that the ice cap formed in response to middle to late Holocene cooling. Deltasø sediments provide an opportunity to assess when in the past North Ice Cap was large enough to dam the glacial lake Gletschersø upstream of Deltasø (Figs. 1 and 2).

2. Methods

2.1. Study site

Deltasø is a 0.3 km^2 through-flowing lake, located at 385 m asl within the presently ice-free land area known as Nunatarsuaq. Nunatarsuaq is bounded to the north and west by the North Ice Cap, to the east by the Greenland Ice Sheet, and to the south by Wolstenholme Fjord and the ice sheet outlet glacier Harald Moltke Bræ (Fig. 1; Greenlandic name Ullip Sermia). North Ice Cap is a major feature of northwest Greenland, with an area of ~1900 km^2, a maximum elevation ~1200 m asl, and numerous outlet glaciers, three of which presently reach the coast. Importantly for this study, part of North Ice Cap drains into Deltasø via the Knud Rasmussen glacier (Greenlandic name Equtissaatsut Sermiat) and the outlet stream of its ice-marginal lake Gletschersø (Figs. 1 and 2). In the past, North Ice Cap meltwater should have reached Deltasø only when the Knud Rasmussen glacier was large enough to dam Gletschersø so that it overflowed to the south (and thus into Deltasø) as it does today. The lakes therefore act as a "threshold lake" system (Briner et al., 2010). Given its landscape position and distance from the modern Greenland Ice Sheet margin, Deltasø has

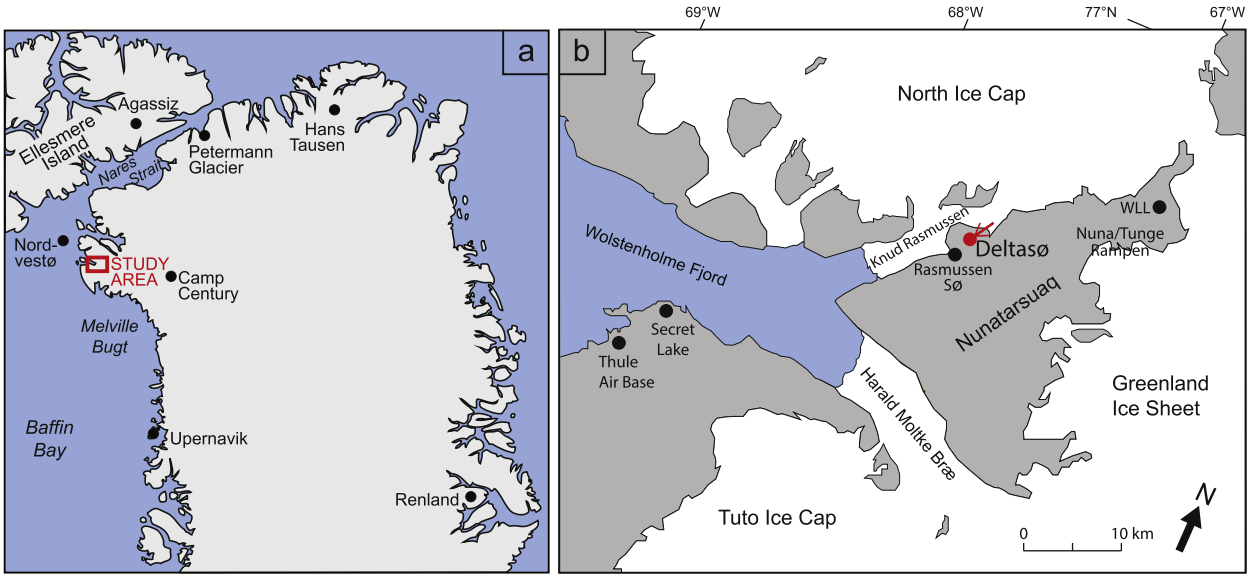

Fig. 1. Location of Deltasø with respect to (a) major features of northern Greenland and nearby paleoclimate study sites, with inset area shown as red rectangle, and (b, inset area) the Thule/Nunatarsuaq region. Red arrow shows routing of ice cap meltwater inflow to Deltasø. Sites of nearby studies at Secret Lake (Lasher et al., 2017), Wax Lips Lake (WLL) (McFarlin et al., 2018) and Nuna and Tunge Rampen (Farnsworth et al., 2018) are also shown. (For interpretation of the references to colour in this figure legend, the reader is referred to the Web version of this article.)

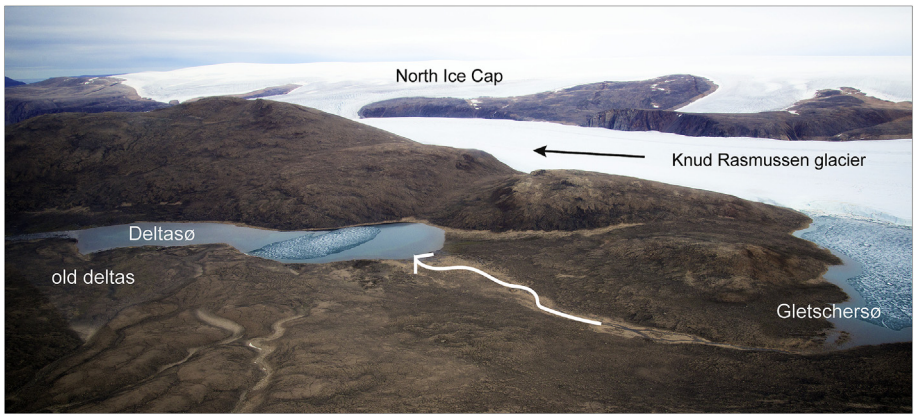

Fig. 2. Oblique aerial view of Deltasø and major nearby landscape features in July 2014. White arrow indicates meltwater inflow from Knud Rasmussen glacier, an outlet of North Ice Cap. Black arrow indicates direction of glacier flow. View toward west-northwest. Photo courtesy Alex P. Taylor.

most likely been isolated from the ice sheet's meltwater since regional deglaciation at the last glacial-interglacial transition.

Most of Nunatarsuaq is underlain by Archaean orthogneiss, with amphibolite dikes of the Thule dike swarm also occurring near Deltasø (Dawes, 1991, 2006; Farnsworth et al., 2018). Middle Mesoproterozoic to late Neoproterozoic sedimentary rocks outcrop in the southernmost part of Nunatarsuaq south of Deltasø and along the western margin of North Ice Cap and likely underlie a large portion of the ice cap (Dawes, 2006; Pedersen et al., 2013). The landscape surrounding Deltasø is mantled by a thin, weathered drift (the Nuna III drift of Farnsworth et al., 2018) deposited by the Greenland Ice Sheet, which flowed from southeast to northwest over Nunatarsuaq during the last glacial period. A series of deltas on the southeastern side of the lake (Fig. 2) were likely deposited during the last deglaciation of the ice sheet. The deltas record inflow from a former outlet of the ice sheet that occupied a valley southeast of Deltasø, and mark higher lake levels that may have been due to damming of Deltasø's outlet by an ice-sheet outlet glacier in the valley now filled with Rasmussen Sø 2.5 km due south of Deltasø. Both the weathered drift and the delta surfaces are cobble- and boulder-rich and are very sparsely vegetated.

Estimated July air temperature at Deltasø for AD 1952–2012 is 6.2 °C. This estimate reflects average July air temperatures for that period measured at the meteorological station at Thule Air Base (Pituffik), 38 km to the southwest at the outer coast, plus the +1 °C difference between July air temperatures measured at the Thule weather station and those measured by our team with a solar-shielded Hobo temperature logger (U23 pro v2) installed at Deltasø throughout July 2013 and 2014. Thule Air Base receives 184 ± 56 mm of precipitation annually (1952–2012), with the majority of precipitation falling in the months of July–October when Northern Baffin Bay sea ice is at a minimum (Wong et al., 2015; Osterberg et al., 2015).

2.2. Field methods

The Deltasø sediment record was captured in three overlapping cores: Core 12-DS-03 was recovered with a Bolivia percussion piston corer from the deepest portion of the lake, at 18.7 m water depth at 76.75952°N, 67.61005°W. The coring site was in the deeper northern sub-basin of the elongate lake, which is also the sub-basin closest to the lake's main inflow (from Gletschersø). Coring for 12-DS-03 intentionally began 20 cm deep in the sediments. The parallel core 12-DS-04 was recovered from 18.7 m water depth a few meters away (at 76.75948°N, 67.61017°W), starting at 120 cm deep in the sediments, to overlap with core 12-DS-03 and penetrate deeper into the stratigraphy. The surface core DS-12-02G was recovered with a Glew gravity corer from 18.6 m water depth nearby (76.75952°N, 67.61002°W). The surface core captured an intact sediment-water interface and was vertically subsampled in the field at 0.25 cm increments for the top 10 cm and at 0.5 cm increments for 10–40 cm depth.

2.3. Indicators of sediment composition

The two overlapping piston cores 12-DS-03 and -04 were split and imaged at the LacCore National Lacustrine Core Facility at the University of Minnesota. Magnetic susceptibility (MS) was measured at LacCore with a Bartington MS3 meter and MS2E sensor mounted to a Geotek MSCL-XYZ. Weight percent biogenic silica (bioSiO_2) was measured at Northwestern's Quaternary Sediment Lab on the Glew core DS-12-02G and the upper piston core 12-DS-03 following the methods for spectrophotometry described by Mortlock and Froelich (1989) but using 10% Na_2CO_3. Average precision (from three duplicates) is 0.44 wt percent bioSiO_2, and the calibration error is 0.05. LOI/TOC datasets from the three cores (and MS measurements from the two piston cores) were spliced together based upon their known depths relative to the sediment-water interface.

For the piston cores, weight percent organic matter in bulk sediment was estimated by loss-on-ignition (LOI) at 550 °C for 2 h (Heiri et al., 2001). For the Glew (surface) core DS-12-02G, and several piston core samples analyzed to provide direct comparison with LOI, weight percent total organic carbon (TOC) and weight percent carbonate were measured by coulometric titration on a UIC Coulometer. Samples were freeze-dried and homogenized before analysis following standard CO_2 coulometric procedures (Huffman, 1977). Carbonate content is negligible, <0.2% in all samples analyzed. Average precision on duplicates is 0.03 wt percent carbonate with a standard deviation of 0.02. The standard deviation of carbonate standards is 0.24 and the standard deviation weight percent TOC of the in-house (Union Springs shale) standard is 0.02. To construct a continuous record of organic carbon content, TOC in piston cores was estimated from LOI based upon overlapping measurements from identical piston core samples, in which TOC ≈ LOI × 0.35. This site-specific observed ratio of TOC:LOI is lower than reported in some classic studies of the LOI method (e.g., 0.47 from Dean (1974)). However, this lower ratio is consistent with prior observations of sediments that have high mineral content and thus may disproportionately lose water from clay lattices and metal

oxides at 550 °C (Heiri et al., 2001; Santisteban et al., 2004; Sutherland, 1998).

Sediment elemental composition was analyzed with an ITRAX X-ray fluorescence (XRF) core scanner at 1 mm resolution and 30 s dwell time, using a molybdenum tube at a power of 30 kV and 20 mA. Scanning XRF analyses of lake sediment cores are affected by sediment properties like water content, organic content and grain size (Davies et al., 2015; Tjallingii et al., 2007), so we interpret XRF results as indicating relative (not quantitative) changes in abundance of elements. XRF analyses were conducted on the upper piston core 12-DS-03, which captured the entire lacustrine section except for the uppermost 20 cm; the uppermost 20 cm were recovered only in the (field-subsectioned) Glew core DS-12-02G, for which an intact core was not available for scanning or photographing. To summarize major trends in elemental abundance, we used principal component analysis (PCA) of all measured elements. Each element was measured as counts per second (cps) and scaled to unit variance but otherwise untransformed. Axis 1 of the PCA explains 27% of the dataset variance, and Axis 2 explains 9%.

2.4. Geochronology

To establish an age model for the uppermost sediments in the surface core, activities of ^{210}Pb were measured using a Canberra high-purity Ge well detector in the Dartmouth Short-Lived Radionuclide Laboratory. Detector calibration followed Landis et al. (2012), with preparation of standards by dilution of reference U-ore BL5 (<1 wt %) with materials spanning the composition/bulk density of sediment core samples. The radionuclides ^{210}Pb, ^{226}Ra and ^{137}Cs were measured using their characteristic gamma emissions at 46, 186 and 662 keV, respectively. The atmospheric or 'excess' component of ^{210}Pb in any depth increment of the sediment core was determined as $^{210}Pb^{excess} = {}^{210}Pb^{total}$ minus $^{210}Pb^{sup}$. Total ^{210}Pb in samples ($^{210}Pb^{total}$) was measured directly by gamma spectrometry. Contribution of $^{210}Pb^{sup}$ by *in situ* decay of geogenic ^{226}Ra was estimated by the asymptote in total $^{210}Pb^{total}$ activity with core depth, but indexed to ^{226}Ra to account for changes in core composition. Thus, $^{210}Pb^{sup}$ at any core depth i was estimated as follows:

$$^{210}Pb_i^{sup} = {}^{226}Ra_i \bullet \frac{^{210}Pb_\infty^{total}}{^{226}Ra_\infty}$$

Here ∞ indicates core depths below the exponential cap in $^{210}Pb^{excess}$, where the $^{210}Pb_{total}/^{226}$Ra ratio approaches a constant value, i.e., a^{210}Pb asymptote. For implementation of $^{210}Pb^{excess}$ chronometry we used the Constant Rate of Supply model (Appleby and Oldfield, 1978) with sedimentation rates and propagated uncertainties following Binford (1990).

Remains of aquatic bryophytes (n = 6) and aquatic invertebrates (chironomid head capsules and cladocera ephippia and carapaces; n = 3) were submitted to WHOI-NOSAMS for target preparation and AMS ^{14}C measurements, and ^{14}C ages were calibrated using Calib 7.1 (Stuiver et al., 2017) and the IntCal 13 calibration curve (Reimer et al., 2013) (Table 1). An age model was generated using the rbacon package in R (Blaauw and Christen, 2018) based upon the ^{210}Pb results and six ^{14}C ages, assuming [prior] accumulation rates of 100 yr/cm. The mean of 6,160,000 iterations was used for data interpretation. Three ^{14}C ages were excluded from age modeling: the two deepest ages due to evidence that they reflect hardwater effects active while the Greenland Ice Sheet still occupied the lake's watershed (as described below in Results) and one inverted Holocene age. We adopt the subdivisions of the Holocene described by Walker et al. (2012), i.e. we define the middle Holocene as extending from 8.2 to 4.2 ka BP.

2.5. Chironomid analyses

Chironomid samples were sieved at 106 μm and hand-picked following standard procedures (Walker, 2001), mounted in Euparal and identified according to Brooks et al. (2007). All reported samples yielded the equivalent of at least 50 whole identifiable head capsules, except for the uppermost sample (top 0–1 cm in an Ekman dredge), which yielded the equivalent of 48.5 whole head capsules. At some depths in the surface core, two adjacent samples were combined to reach these sample sizes.

July air temperatures were modeled using two independently developed chironomid training sets from northeastern North America (Fortin et al., 2015; Francis et al., 2006). Among published chironomid training sets, these are the most climatically and biogeographically relevant to northwest Greenland over the Holocene. One training set includes 434 sites representing a July air temperature gradient from 2.0 to 16.3 °C and spanning from Boreal to High Arctic environments, including the Canadian Arctic islands (from Fortin et al. (2015), hereafter FOR15). The FOR15 training set was used with a two-component weighted averaging partial-least-squares (WA-PLS) model (78 taxa, $r^2_{boot} = 0.72$, RMSEP = 1.9 °C). The second training set incorporates 68 different sites located from Maine, USA, to the Canadian Arctic islands, including sites on Devon Island ~500 km west of Deltasø, and representing July air temperatures from 5 to 19 °C (from Francis et al. (2006); Walker et al. (1997), hereafter FRA06). The FRA06 training set was used with a weighted averaging (WA) model employing tolerance down-weighting and inverse deshrinking (44 taxa, $r^2_{jack} = 0.88$, RMSEP = 1.5 °C).

A limitation of using the FRA06 calibration data and a WA model for reconstructing temperatures at Deltasø is that the training set contains few sites colder than Deltasø is at present. Colder past periods therefore fall near or beyond the edge of the training set temperature gradient. This is likely to result in overestimation of modeled temperatures during the coldest periods (Axford et al., 2017; Juggins and Birks, 2012). Therefore, for periods when chironomid assemblages from Deltasø show qualitative evidence for colder-than-present temperatures, we assume that paleotemperatures modeled using FRA06 should be viewed as *maximum* temperatures – and thus the inferred temperature *difference* between the warmest and coldest times is a *minimum* estimate. We cannot rule out that temperature modeling with FOR15 may also be affected by the same problem, but the colder calibration sites in that model mean that it should perform better at colder temperatures.

Temperature modeling was conducted using the software package C2 v. 1.7.7 (Juggins, 2007). Species data were square-root transformed for both models, and rare taxa (defined as taxa with maximum abundance <2%) were excluded from temperature modeling. The following taxa were lumped for temperature modeling to harmonize with the training set taxonomy: all Tanytarsini were lumped for the FRA06 model (whereas *Micropsectra* and *Corynocera oliveri/Tanytarsus lugens* type were subdivided for use with FOR15), and for both models all Pentaneurini and *Psectrocladius* morphotypes were lumped. All identified subfossil taxa are represented in the FOR15 training set except *Trissocladius*, which was found in two downcore samples both at abundance <1%. Several minor subfossil taxa are not represented in the FRA06 training set (*Paracladopelma, Rheotanytarsus, Cladotanytarsus, Metriocnemus, Chaetocladius, Rheocricotopus, Paracricotopus, Brillia, Trissocladius* and *Pseudosmittia*). Of those taxa only *Metriocnemus* (present in three samples at abundances up to 1.9%) is present in more than two downcore samples, and only *Cladotanytarsus*

Table 1
Radiocarbon results from Deltasø.

<!––Col Count:11 ––>NOSAMS Accession #	Core ID	Depth in core sediment (cm)	Depth below sediment –water interface (cm)	Material dated	Fraction Modern[a]	FM error	Measured $\partial^{13}C$ (‰)	^{14}C Age (^{14}C yr BP)	Calibrated age[c] (cal yr BP ±2σ)	Calibrated age (median)
OS–108018	DS –12 –03	1 cm	21 cm	aquatic plant macrofossils	0.8260	0.0030	-23.86	1530 ± 30	1440 ± 90	1420
OS–108450	DS –12 –03	6–8 cm	26–28 cm	aquatic plant macrofossils	0.6749	0.0033	-29.13	3160 ± 40	3360 ± 100	3387
OS–108451	DS –12 –03	11–13 cm	31–33 cm	aquatic plant macrofossils	0.6989	0.0028	-25.46	2880 ± 30	3010 ± 130	3006
OS–102751	DS –12 –03	28–34 cm	48–54 cm	aquatic plant macrofossils	0.5682	0.0020	-28.45	4540 ± 30	5190 ± 120	5156
OS–102626	DS –12 –03	60–64 cm	80–84 cm	aquatic plant macrofossils	0.5048	0.0031	-26.85	5490 ± 50	6300 ± 100	6292
OS–108185	DS –12 –03	95 cm	115 cm	aquatic plant macrofossils	0.3812	0.0025	-25.94	7750 ± 55	8520 ± 100	8524
OS–134709	DS –12 –03	107–109 cm	127–129 cm	aquatic invertebrate remains	0.3517	0.0018	-29.03	8400 ± 40	9400 ± 100	9440
OS–102753	DS –12 –04	16–22 cm	136–142 cm	aquatic invertebrate remains	0.2125	0.0026	-28.17	12,450 ± 100[b]	14,610 ± 450[b]	14,596[b]
OS–102630	DS –12 –03	118–124 cm	138–144 cm	aquatic invertebrate remains	0.2083	0.0113	-28.37	12,600 ± 440[b]	14,850 ± 1270[b]	14,856[b]

[a] FM values require no further correction for fractionation.
[b] Ages from the basal unit are inferred to incorporate significant old carbon and thus not to represent true stratigraphic age.
[c] Reported as the midpoint ± half of the 2σ calibrated age range, with values rounded to the nearest ten years.

(present in one sample at 3.3% abundance) achieves an abundance of 2% or more. To formally assess the quality of training set analogs to our fossil assemblages, we calculated squared chord distances (SCDs) between each complete, untransformed fossil assemblage and its closest modern analogue in each training set using the modern analog technique (MAT).

3. Results

3.1. Sediment stratigraphy, composition and geochronology

3.1.1. Deglacial stratigraphy and depositional history

The basal unit of the Deltasø cores is a stony, compacted diamicton from 192 to 166 cm, overlain by a sharp contact with a minerogenic sand unit from 166 to ~145 cm (Fig. 3). The sand grades into an overlying ~145-cm-thick unit of laminated light to medium tan (yellowish brown) lacustrine mud which continues to the top of the record (although detailed stratigraphy is not known for the uppermost 20 cm, captured only the field-subsectioned Glew surface core). Darker gray laminae are most common in the lower part of the lacustrine unit below 127 cm depth. The basal diamicton unit is characterized by high and variable MS, and LOI values averaging 8–9% (equivalent to TOC ~3%). These LOI values are lower than in the lacustrine mud, but surprisingly high for sediments we interpret as till. This likely reflects high clay-water content in the diamicton, and may also suggest that organic materials from prior non-glacial periods were reworked into the diamicton by the advancing Greenland Ice Sheet during the last glacial period. The sand unit is distinguished in the proxy data by very low LOI (<1%) and generally very high MS, with MS values declining across the upper gradational contact with the lacustrine mud. The diamicton and overlying sand are interpreted as recording subglacial and proglacial environments, respectively, of the Greenland Ice Sheet as it retreated from the Deltasø watershed.

In the upper portion of the sand unit – the only part of the sand or diamicton units for which we have XRF data – calcium (Ca) and strontium (Sr) are up to five times greater in relative abundance than in the overlying lacustrine sediments (Fig. 3). This contrasting elemental composition of the sand compared with all parts of the overlying fine-grained lacustrine unit (summarized by PCA Axis 2 scores, and notably including elevated Ca and Sr abundance; Figs. 3 and 4) is consistent with a very different sediment provenance. That, in turn, is consistent with sourcing of the sand from the Greenland Ice Sheet, which would have transported exotic materials to the lake's watershed from a large subglacial region and deposited sand in the lake via proglacial meltwater streams until the ice sheet retreated out of Deltasø's watershed. Sediment elemental composition remains distinguishable from the overlying sediments up to a depth of ~140 cm, suggesting continued influence of ice-sheet derived sediments up to that depth.

The two deepest ^{14}C ages obtained, from aquatic materials 136–144 cm depth (Table 1), are anomalously old, predating all published evidence for regional deglaciation by several thousand years (Corbett et al., 2015; Farnsworth et al., 2018). These ages come from the zone of somewhat elevated Ca at the base of the fine-grained lacustrine sediments (Fig. 3), which we (above) interpret as evidence for the final stages of ice sheet meltwater influence on the lake. We infer that influx of Ca-rich sediments and/or of ancient Greenland Ice Sheet meltwater to the lake during deposition of these sediments created a hardwater effect that makes aquatic organic materials from these oldest lacustrine sediments date erroneously too old. Therefore, we do not include the two ages from this unit in our age model below.

3.1.2. Holocene lacustrine sediments and geochronology

Modeled sedimentation rates within the lacustrine unit

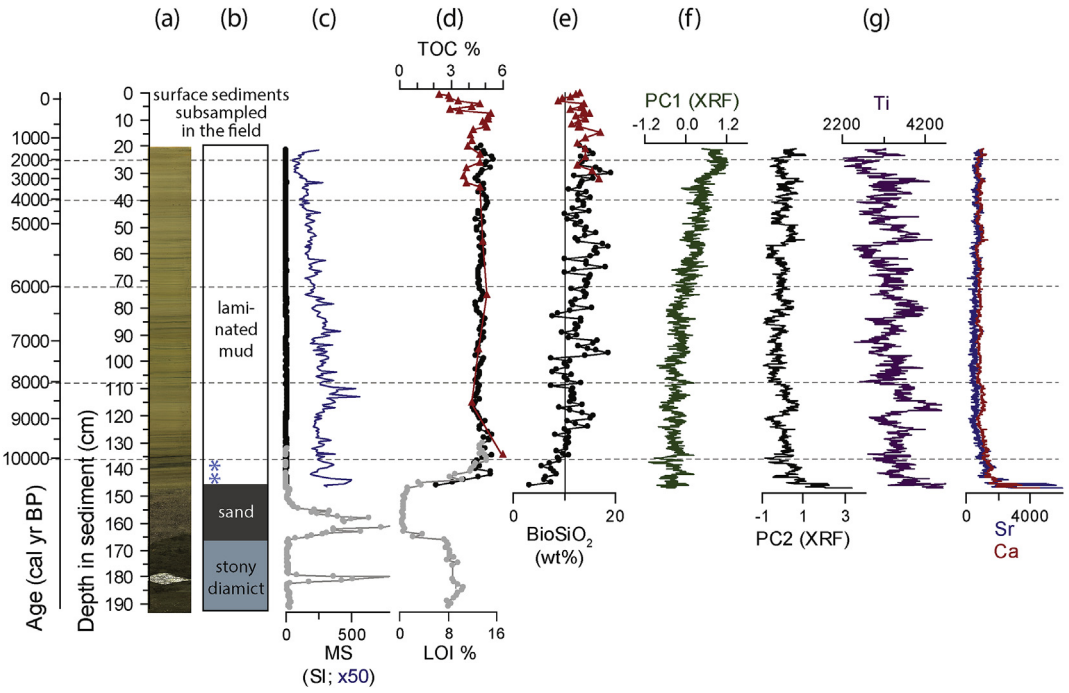

Fig. 3. Summary of Deltasø core stratigraphy and sediment composition, including (a) core photograph; (b) summary of stratigraphic units, with depths of rejected pre-Holocene ages shown as blue stars; (c) magnetic susceptibility (MS, with blue curve magnified × 50); (d) percent total organic carbon (TOC), as measured by coulometer and elemental analyzer (red) or estimated from loss on ignition (0.35 × %LOI, black and gray); (e) biogenic silica (bioSiO$_2$); (f) first and second principal components from PCA of XRF results, summarizing trends in elemental abundances; and (g) Ti, Sr and Ca counts per second from XRF. MS and LOI data from overlapping lower piston core 12-DS-04 are in light gray and TOC and bioSiO$_2$ data from the upper piston core 12-DS-03 are in black (except for overlapping TOC measurements on five widely spaced piston core samples, in red with higher-resolution surface core TOC). (For interpretation of the references to colour in this figure legend, the reader is referred to the Web version of this article.)

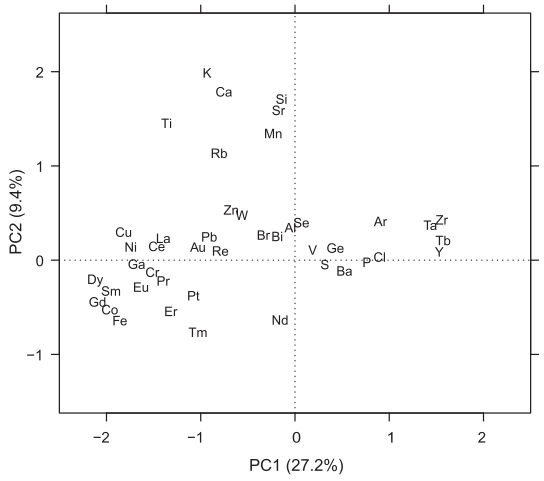

Fig. 4. Elemental species (variable) scores from principal component analysis (PCA). Labels are standard abbreviations for elements. Axis labels include percent of variation explained.

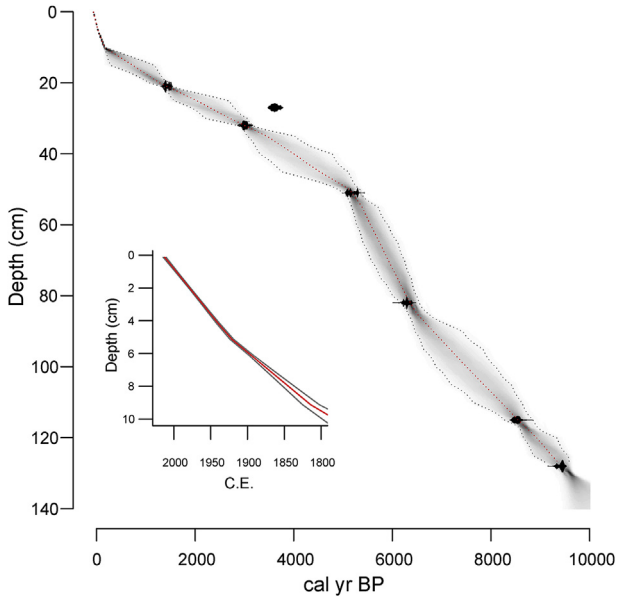

Fig. 5. Age model for Deltasø sediments, based upon ^{210}Pb and ^{14}C ages. Probability density functions (shaded) are bounded by 95% confidence intervals (gray lines), with red curve showing the single 'best' model from 6,160,000 iterations. The rejected late Holocene age is shown here, and the stratigraphic positions of rejected >14.5 ka BP ages are shown in Fig. 3. See Table 1 for ^{14}C results. (For interpretation of the references to colour in this figure legend, the reader is referred to the Web version of this article.)

decrease by a factor of two after ~5.2 ka BP, and apparent (wet) sedimentation rates increase again in the upper 10 cm of the record (Fig. 5). The latter shift may partly reflect less compaction and thus higher water content in the uppermost sediments, and the apparent abruptness of the change may be an artifact of joining the ^{210}Pb and ^{14}C chronologies at that depth. However, given the magnitude of the change in modeled sedimentation rate there is also likely a real increase in sediment flux reflected in the upper 10–20 cm of sediment. Ninety-five percent confidence bands for the ^{14}C-constrained portion of the age model range yield uncertainties of ± <200 yr (near age controls) to ± >500 yr (between ^{14}C dates and around changes in sedimentation rate), and in the ^{210}Pb-constrained upper sediments two-sigma uncertainties

range from ±2 yr (in the past ~50 yr) to ± 20–25 yr (in the early 19th century).

MS and titanium (Ti) abundance broadly covary on sub-millennial timescales throughout the upper laminated lacustrine unit, consistent with minerogenic content being the primary signal recorded by both proxies within this unit (Fig. 3). Despite this sub-millennial variability, there is only a small and gradual long-term, multi-millennial trend in these parameters, with MS and Ti both decreasing slightly overall from the early to late Holocene. Similarly, PC2 from the PCA reflects sub-millennial variations but no long-term shift in abundance of Ti or other rock-forming elements (including Ca, K, Si, Mn, Sr; Figs. 3 and 4). PC1 is defined primarily by elements (e.g., zirconium (Zr), yttrium (Y), terbium (Tb) and tanalum (Ta)), mostly rare, that appear for the first time after 5.8 ka BP (e.g., Tb) or rise throughout the subsequent middle to late Holocene (e.g., Ta, Zr). The new occurrence or rise of these minor elements after 5.8 ka BP could reflect a change in provenance of minerogenic sediments (e.g., perhaps new influx of windblown material from the Neoproterozoic sedimentary terrane near the current North Ice Cap); however, lower sedimentation rates (Fig. 5), relatively unchanged organic content and higher average bioSiO_2 concentrations (Fig. 3) in the late Holocene compared with the early Holocene indicate that this source must have been small in quantity. Lack of corresponding rise in Ti or MS is evidence against a corresponding increase in clastic input derived from the local orthogneiss bedrock. We do not have MS or XRF scan data for the uppermost 20 cm of the record because the surface core was subsampled in the field.

Organic content is remarkably steady through most of the lacustrine unit, except near its base where LOI values rapidly rise from ~3 to 15% (equivalent to ~1–5% TOC), and after 1850 AD when TOC drops to <3%. (Figs. 3 and 6). BioSiO_2 rises from ~3 to 12% within the bottom 10 cm of the ~145-cm-thick lacustrine unit, and stays above 10% for most of the overlying section. This parameter shows significant sub-millennial variability but generally highest values between ~7.5 and 3 ka BP. Minimum late Holocene bioSiO_2 values occur in the early to mid-20th century AD.

3.2. Chironomids

Assemblages at Deltasø are dominated by taxa associated with cold, oligotrophic, well-oxygenated environments. The most common subfamilies are Tanytarsini, including *Micropsectra*, and Orthocladiinae, especially *Heterotrissocladius* and *Oliveridia/Hydrobaenus* (Fig. 6). *Sergentia*, with a maximum abundance <9%, is the only common member of the Chironomini. Tanypodinae are present in some samples, but at low abundance (<4%).

The earliest assemblages, prior to ~10 ka BP, were >90% Tanytarsini and contained the record's highest abundances of *Tanytarsus lugens/Corynocera oliveri*, which have been associated with early colonization of Canadian Arctic sites immediately after deglaciation (Saulnier-Talbot and Pienitz, 2010). There was an overall trend throughout the early to middle Holocene of decreasing Tanytarsini and increasing *Heterotrissocladius* (Fig. 6). The coldest stenotherm in the assemblage, *Oliveridia/Hydrobaenus*, first became abundant ~5.4 ka BP, and was most abundant in the past 1.5 kyr. Additional taxa with relatively low temperature optima also increased in abundance in the late Holocene: *Sergentia* was most abundant in the middle to late Holocene and *Eukiefferiella* was most consistently present after 4.0 ka BP. *Cricotopus/Orthocladius* were rare (<2%) until 2.0 ka BP. Two taxonomic groups more associated with higher temperatures at arctic sites show trends inverse to *Oliveridia/Hydrobaenus*: Tanypodinae were often present prior to 5.7 ka BP, but mostly absent (present in only one sample) after that. Similarly, *Psectrocladius* was commonly present prior to 5.7 ka BP, but was very rare later. The last ~75 yr (since ~1940 AD) were unique within the late Holocene, characterized by the rise of *Cricotopus/Orthocladius* and Tanytarsini, including *Micropsectra*, decline of *Oliveridia/Hydrobaenus* and *Heterotrissocladius* and loss of *Sergentia*.

Reconstructed temperature trends clearly reflect the species changes described above, with higher-than-present temperatures reconstructed for the early to middle Holocene and highest temperatures ~10 to 6.2 ka BP (Fig. 6). Estimates of HTM temperature anomalies vary by ~1 °C between FRA06 vs. FOR15, with FRA06 yielding higher temperature estimates for many but not all samples. During the warmest period, hereafter referred to as the local Holocene Thermal Maximum (HTM), inferred July air temperatures were 2–3.5 °C warmer than modern (as compared with modeled temperatures from a surface sample taken from 0 to 1 cm) and *at least* 3–3.5 °C warmer than the coldest part of the late Holocene (temperatures from the coldest period appear "too cold to quantify," as described below). We reiterate that these HTM temperature anomalies could be underestimates, given the potential – per Methods and as further discussed below – for late Holocene (including surface sediment) assemblages to yield overestimated temperature reconstructions.

Cooling after the HTM began ~6.2 ka BP according to both temperature models. After 5.4 ka BP, modeling with FOR15 suggests progressive cooling to minimum temperatures in the last millennium. In contrast, for FRA06 the flat temperature reconstruction throughout this period (despite significant changes in the chironomid assemblage, including changes in temperature-sensitive taxa like *Oliveridia/Hydrobaenus*) reflects the known limitation (discussed in Methods) of using this training set and a weighted-averaging model for very high-latitude reconstructions during periods colder than today. MAT results further support the relative robustness of FOR15-derived temperature estimates for the late Holocene over those from FRA06: All downcore assemblages have good analogs (defined as SCD less than the 5th percentile within the training set) in the FOR15 training set. In the FRA06 training set, 27% of downcore samples (all within the late Holocene or initial deglacial period) had nearest analogs with SCDs greater than the 5th percentile, including 12% with SCDs exceeding the 10th percentile. In other words, FRA06 offers good analogs for assemblages from periods warmer than today, but poor analogs for cooler periods. The same was observed at nearby Wax Lips Lake 20 km northeast of Deltasø; Fig. 1; McFarlin et al. (2018). In recognition of these problems, we hereafter characterize temperatures after 5.4 ka BP at Deltasø as "too cold to quantify using FRA06."

4. Discussion

4.1. Local Greenland Ice Sheet and North Ice Cap history

Collectively, evidence from Deltasø and surrounding sites indicates that the Greenland Ice Sheet deglaciated from the lake basin between 10.8 and 10.1 ka BP. The deepest reliable ^{14}C age obtained from Deltasø is 9.4 ka BP, but this date is from 10 cm above a gradational contact with sand deposited by ice sheet meltwater. Thus, 9.4 ka BP is a minimum-limiting age for deglaciation but probably not a close minimum-limiting age given its stratigraphic position. The oldest Holocene ^{14}C ages from nearby Wax Lips Lake (Fig. 1) are 10.1 and 10.0 ka BP (McFarlin et al., 2018), providing minimum-limiting ages for deglaciation at a site 15–20 km inboard of and at higher elevation than Deltasø. ^{14}C ages of shells and seaweed in raised marine deposits indicate that the coast of inner Wolstenholme Fjord was deglaciated by 10.3 ka BP (as summarized by Farnsworth et al. (2018)). Although ^{10}Be inheritance in boulders and bedrock on the Nuna III drift has prevented a precise determination of deglaciation in Nunatarsuaq (Farnsworth et al., 2018),

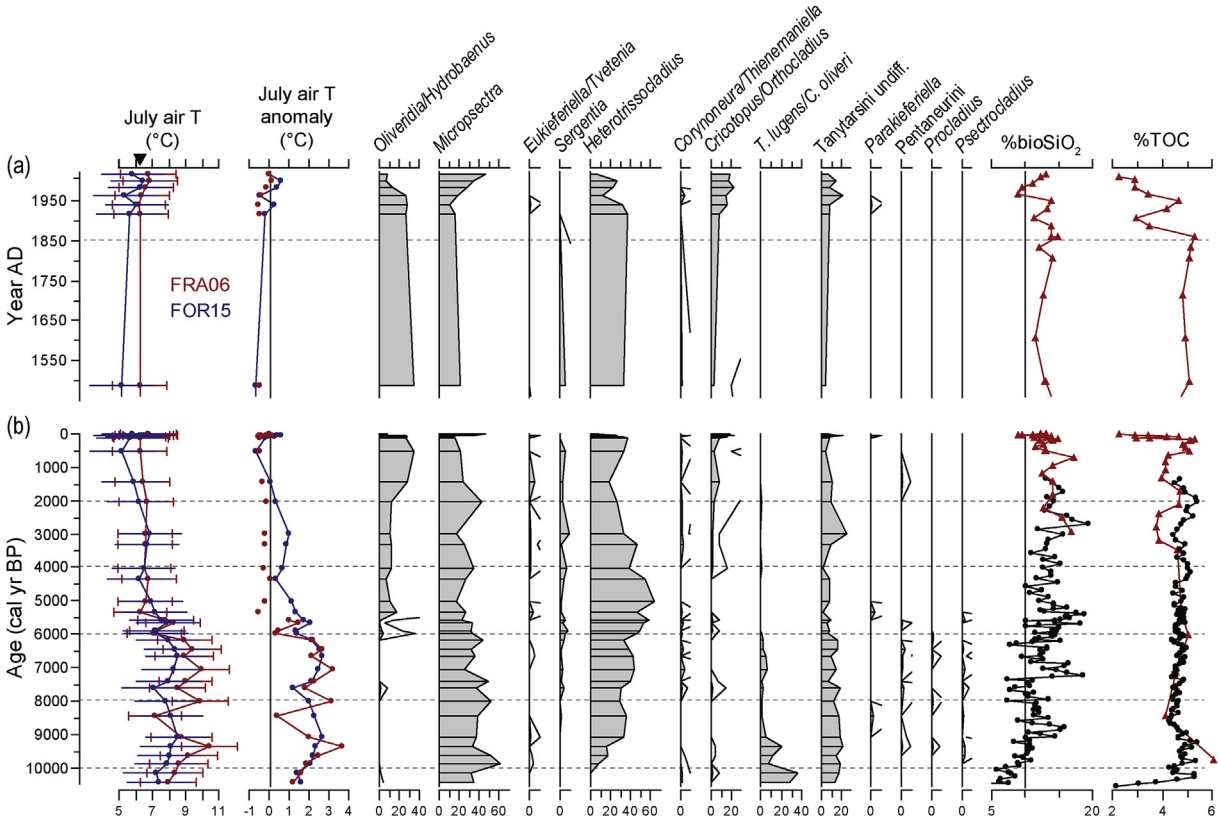

Fig. 6. Holocene chironomid, bioSiO$_2$ and TOC data from Deltasø, with (a) showing details since 1450 AD and (b) showing the entire chironomid record. Chironomid-inferred July air temperatures and temperature anomalies are modeled using two independent training sets and transfer functions (FOR15 vs. FRA06). Error bars show bootstrapped sample-specific errors, and inverted black triangle shows instrumental modern July air temperature. Temperature anomalies are relative to the surface sample. For the period considered "too cold to quantify" with the FRA06 transfer function, temperature anomalies are shown as points not connected by lines. Percentages are shown for chironomid taxa occurring at abundances >2% in at least two samples, with taxa ordered approximately by temperature optimum (left = cold) and with the same x-axis scaling for all taxa. Unfilled lines are 10 × exaggerations. Black circles are data from the piston core (for bioSiO$_2$) and estimated from LOI (for TOC).

Corbett et al. (2015) used ^{10}Be in boulders to infer that the landscape around Thule Air Base was deglaciated by ~10.8 ka BP. Corbett et al. (2015) also inferred a subsequent major advance of Harald Moltke Bræ in the early Holocene, but Farnsworth et al. (2018) summarized a range of evidence arguing against that interpretation. The lack of a spike in Ca abundance, coarse grain size or any dramatic increase in minerogenic content (as inferred from Ti or MS) above the deglacial transition in Deltasø indicates that the Greenland Ice Sheet never returned to Deltasø's watershed after deglaciation.

Preservation of inorganic, minerogenic lacustrine units is widely used as an indicator of Holocene glacial input to lakes around Greenland (Briner et al., 2010; Larsen et al., 2017; Levy et al., 2014). Deltasø lacks such units between regional deglaciation ~10.8-10.1 ka and ~AD 1850, as evidenced by the consistent appearance, LOI, bioSiO$_2$, and inferred minerogenic content (MS, Ti, PC2) of the sediments in this zone, as well as low sedimentation rates (Figs. 3 and 5). Based upon this observation, we rule out periods of meltwater influx from nearby North Ice Cap prior to the last ~165 years. Increases in several rare elements (summarized by PC1; Figs. 3 and 4) after 5.8 ka BP may record addition of new bedrock type(s) to the lake's sedimentary provenance but do not correspond with indicators of minerogenic content or increasing sedimentation rates, so do not suggest glaciofluvial input.

After 1850 AD, TOC dropped to the lowest values since regional deglaciation and bioSiO$_2$ reached the lowest values of the late Holocene (Fig. 6). We infer expansion of Knud Rasmussen glacier at ~1850 AD to a configuration that dammed Gletschersø, causing overflow of meltwater and influx of minerogenic glacial sediments to Deltasø. The flux of glacial sediments to Deltasø during this time was likely small. During field work we observed little-to-no suspended sediment (i.e., rock flour) in the meltwater streams that drain North Ice Cap today, as well as in its modern ice-marginal lakes, suggesting that the ice cap is not currently eroding its base. Additionally, the presence of only a thin drift proximal to the ice-cap margin suggests that the ice cap was likely cold-based during its recent maximum extent. Nonetheless, glaciogenic sediment flux to Deltasø between ~1850 AD and present was enough to dilute TOC and bioSiO$_2$ and simultaneously increase overall sedimentation rates (Figs. 5 and 6). Deltasø still receives meltwater from North Ice Cap today, consistent with low TOC in the lake's surface sediments (Fig. 6).

Previous evidence for Holocene fluctuations of independent ice caps in northwest Greenland indicates that they were less extensive than today for at least part of the Holocene; but that evidence is limited. Reeh et al. (1990) concluded that the absense of Pleistocene ice (ice with strongly negative δ^{18}O signatures) in a sample transect from the Tuto Ice Cap ramp (~40 km south of Deltasø and North Ice Cap; Fig. 1) indicated that the Tuto Ice Cap disappeared in the early Holocene. Goldthwait (1960) hypothesized that North Ice Cap grew through the late Holocene. Our results from Deltasø are broadly consistent with these inferences regarding nearby ice caps, and with reconstructed Holocene temperature changes described in the section below. North Ice Cap's history is also notably similar to that of the much larger Flade Isblink in north Greenland, where outlet glaciers were smaller than today from ~9.4 to 0.2 ka BP (Larsen

et al., 2019).

The Greenland Ice Sheet also retracted during the HTM and expanded in the middle to late Holocene around northwest Greenland. Exceptional early Holocene thinning of up to 1 km has been inferred at the Camp Century drill site ~175 km northeast of Deltasø (Fig. 1), although that inference is only supported by models when a large HTM temperature anomaly is imposed (Lecavalier et al., 2017; Vinther et al., 2009). Marine shells sheared up at the margin of the ice sheet outlet glacier Harald Moltke Bræ date to 7.8 ka BP, and record a time when part of the upstream fjord must have been ice-free (Mörner and Funder, 1990). Farnsworth et al. (2018) recently ^{14}C-dated subfossil plants recovered from a shear plane within the ice sheet margin in Nunatarssuaq near Wax Lips Lake. The plants date to 4.7 ka BP, recording a time when the land-based ice sheet margin was less extensive. The nearby Nuna and Tunge Rampen (lobes of the land-based ice sheet; Fig. 1) advanced to a maximum Holocene extent between 3.2 and 2.1 ka BP, but most of the land-based margin reached its maximum Holocene extent in the last millennium and likely in the last few hundred years (Farnsworth et al., 2018). Petermann and Humboldt glaciers (marine-terminating ice-sheet outlets) ~450 km north of Nunatarssuaq reached their maximum or near-maximum late Holocene extents in the last few hundred years and, intriguingly, ^{10}Be data suggest that Petermann Glacier also experienced an equivalent late Holocene advance before 2.8 ka BP (Bennike, 2002; Reusche et al., 2018).

4.2. Timing of Holocene temperature shifts in northwest Greenland

Reconstructed summer temperatures at Deltasø based on chironomids were warmer than present at the onset of non-glacial sedimentation at the lake, prior to 10 ka BP and perhaps as early as 10.8 ka BP. Deltasø experienced the warmest summer temperatures of the Holocene between ~10 and 6.2 ka BP, followed by progressive cooling that culminated in the lowest temperatures and maximum ice cap size during the last few centuries (Fig. 7). Lower sedimentation rates at Deltasø between ~5.2 and ~0.5 ka may record lower lake and landscape productivity. Although relative abundances of bioSiO_2 and TOC did not drop, lower sedimentation rates suggest that the absolute fluxes of these biogenic materials may have declined.

When modeling paleotemperatures from paleoecological proxy data, it is essential to consider secondary environmental gradients that may have driven assemblage changes over time (Brooks et al., 2012; Juggins, 2013; Velle et al., 2010). Changes in lakewater oxygenation, lake substrate and macrophyte cover, and watershed soils and vegetation and resulting changes in nutrient cycling and lakewater pH can all affect chironomid assemblages (Anderson et al., 2008; Heggen et al., 2010; Kaufman et al., 2012). Importantly, the current study site bears evidence of relatively little change in these factors through the Holocene. Vegetation and soil development have both been minimal in the crystalline terrain and harsh Mid Arctic climate of Deltasø's rocky, very sparsely vegetated watershed (Fig. 2). In this climate, shallow dilute oligotrophic lakes like Deltasø also tend to be well oxygenated. The organic content (LOI/TOC) of Deltasø sediments and inferred primary production (bioSiO_2) varied only moderately through the Holocene (Fig. 3), and not in concert with major shifts in chironomid assemblages. Thus, this site seems a good candidate for avoiding most problematic secondary gradients, similar to observations of unproductive arctic lakes in Canada (Medeiros et al., 2015) and in a comparable Mid Arctic environment in East Greenland (Axford et al., 2017). An exception for Deltasø is that in the past ~165 yr ice cap meltwater could have affected chironomid species assemblages by making the lakewater colder or more turbid. Although we cannot rule out some effect from ice cap meltwater on the chironomid fauna, we suggest these effects were minimal: past fluxes of glaciogenic sediments were likely low, given our observations of the modern system (see above); and because the glacier is quite distant from Deltasø, meltwater could warm significantly as it traveled to the lake, which itself would be cool during summer even without meltwater input. At nearby Wax Lips Lake, a smaller lake with no modern glacial meltwater input, we measured with Hobo loggers a mean summer (June, July and August 2013) near-surface water temperature of 5.5 °C.

Historic July air temperatures (estimated to be 6.2 °C at Deltasø for AD 1952–2012) and the modeled temperature for the surface sample (6.8 °C with FRA06 and 5.8 °C with FOR15) agree within model error, supporting the utility of chironomids as a proxy for July air temperatures at this site (Fig. 6), although not necessarily ruling out that FRA06 overestimates temperatures in the surface sample as for other late Holocene samples. Reconstructions of absolute temperature agree reasonably well between models, despite the models' different underlying mathematics and independent training sets. Although temperatures inferred using the FRA06 model are ~1 °C higher than those inferred using FOR15 during the early Holocene and the coldest part of the late Holocene, this difference is well within model error and for at least parts of the late Holocene is probably explained by the aforementioned problem of temperatures that are "too cold to quantify."

Existing terrestrial paleoclimate archives from the surrounding region provide strong support for the temperature trends reconstructed from chironomids at Deltasø, including evidence for warmer-than-present summers starting very early in the Holocene, cooling summers and expanding glaciers after ~6 to 5 ka BP, and lowest temperatures in the last millennium (Fig. 7). In northern Nunatarsuaq (Fig. 1), Holocene chironomid-inferred July temperatures were warmest at Wax Lips Lake between ~10 and 8 ka BP (McFarlin et al., 2018). The sediment record from Secret Lake, ~35 km southwest of Deltasø near Thule Air Base, records a long-term decline in the δ^{18}O of warm-season precipitation, interpreted as cooling temperatures, between 7.7 ka BP (the beginning of record) and the last millennium of the Holocene (Lasher et al., 2017). The highest temperatures at Secret Lake are inferred from the start of that record until 6.3 ka BP, and the lowest temperatures occurred during the last millennium (Figs. 1 and 7). Marine shells transported by Harald Moltke Bræ record ice-free conditions at 7.8 ka BP in part of the fjord currently occupied by the large ice sheet outlet glacier (Mörner and Funder, 1990). As mentioned above, Reeh et al. (1990) suggested the Tuto Ice Cap <50 km south of Deltasø was absent during the HTM, and Goldthwait (1960) inferred that North Ice Cap expanded after 5.4 ka BP. The Greenland Ice Sheet margin near Wax Lips Lake was inboard of its present position at 4.7 ka BP and subsequently expanded (Farnsworth et al., 2018).

The majority of proxy records from the larger region also support peak warmth early in the Holocene. Oxygen isotopes of ice in Agassiz Ice Cap, when corrected for changes in regional landscape elevation over time, imply the warmest annual temperatures of the Holocene occurred from ~11 to 8 ka BP (Lecavalier et al., 2017; Vinther et al., 2009). Melt layers in Agassiz ice suggest peak summer temperatures in the earliest Holocene prior to 10 ka BP, and elevated but declining summer temperatures until ~8 ka BP. Extralimital thermophilous species are recorded in lake sediments from northwest Greenland (fish and beetles; Fredskild (1985)) and island peats of Nordvestø (puffins; Bennike et al. (2008)) <150 km northwest of Deltasø between 8.8 and 5.1 ka BP (Figs. 1 and 7). Gajewski's (2015) recent quantitative reinterpretation of pollen data from several lakes in north/northwest Greenland and Ellesmere Island suggests later onset of regional warmth (~7.2 ka BP),

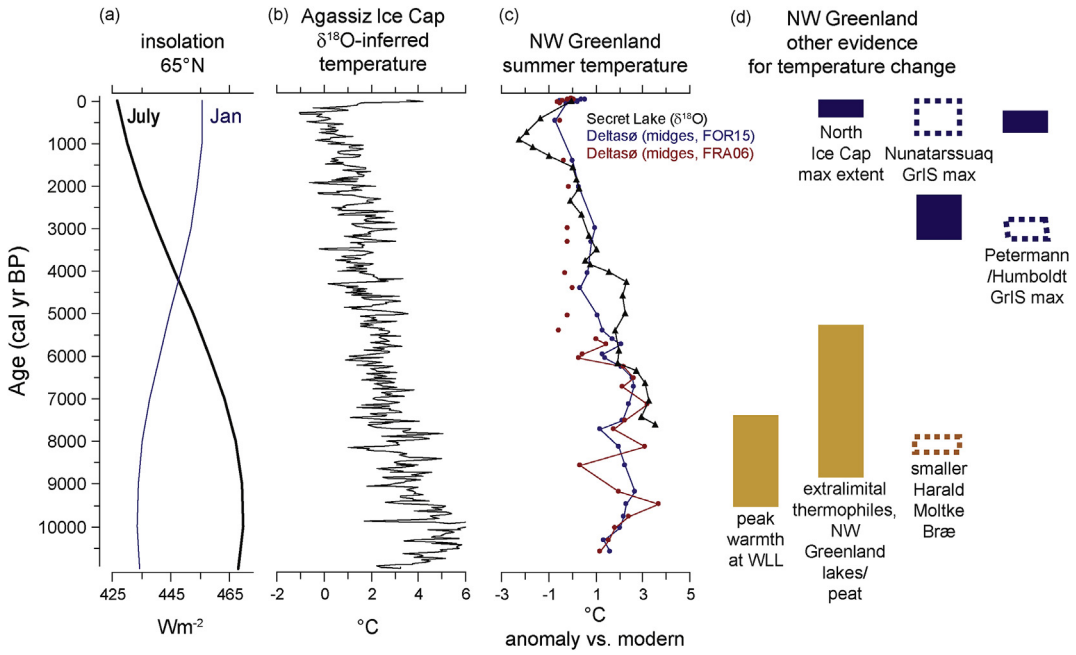

Fig. 7. Evidence for Holocene temperature trends around northwest Greenland. (a) Insolation at 65°N in July and January (Berger and Loutre, 1991). (b) Precipitation-weighted (annually integrated) temperatures inferred from $\delta^{18}O$ of ice at Agassiz Ice Cap, Ellesmere Island (Lecavalier et al., 2017). (c) July air temperature anomalies at Deltasø (red and blue) and chironomid $\delta^{18}O$-inferred summer temperature anomalies from nearby Secret Lake (black; the intermediate of three models from Lasher et al. (2017)). Anomalies are calculated relative to inferences from surface sediments. For the period considered "too cold to quantify" with the FRA06 transfer function, data points are not connected by lines. (d) Other evidence for air temperature changes over northwest Greenland, including: timing of maximum Holocene warmth inferred from chironomids at Wax Lips Lake (WLL) (McFarlin et al., 2018); occurrence of extralimital thermophilous species in peat deposits of Nordvestø (Bennike et al., 2008) and coastal lakes in northwest Greenland (Fredskild, 1985); maximum extent of North Ice Cap, inferred from lake sediments in this study; and late Holocene reduced (orange) and maximum or near-maximum (blue) extents of the Greenland Ice Sheet (GrIS) in Nunatarssuaq (Farnsworth et al., 2018; Mörner and Funder, 1990) and at the Petermann and Humboldt outlet glaciers (Reusche et al., 2018). Dashed lines reflect uncertain timing. Site locations are shown in Fig. 1. (For interpretation of the references to colour in this figure legend, the reader is referred to the Web version of this article.)

but is in agreement with other regional records in indicating cooling beginning at 5.2 ka BP and intensified cooling after 1.8 ka BP. Proxy-to-proxy differences in the apparent timing of the HTM could be attributable to the contrasting seasonal sensitivities of various proxies, site-specific environmental changes that confound proxy responses to temperature change, or (where peak warmth inferred from pollen lags peak warmth inferred from other proxies; e.g., Shala et al. (2017)) lags between postglacial warming and vegetation colonization. The latter effect, though its importance is debated, would support treating pollen records from formerly glaciated regions as providing minimum constraints on the timing of onset of postglacial warmth (Funder, 1978; cf. Gajewski, 2015).

Marine records surrounding northwest Greenland also show evidence for early Holocene warmth and late Holocene cooling. The largely marine-based Greenland Ice Sheet margin around Upernavik ice stream on Melville Bugt retreated to inboard of its current position by ~9.6 ka BP (Briner et al., 2013). Proxies from marine sediments in northern Nares Strait indicate reduced sea ice cover and high marine productivity from 9 to 6 ka BP (Jennings et al., 2011), and Bennike (2002) documented a subarctic extralimital bivalve species off Washington Land ~7.3 ka BP. Fjord sediments from the Arctic coast of Ellesmere Island indicate the Ward Hunt ice shelf did not form until 4 ka BP (Antoniades et al., 2011). Close to our study area in southernmost Nares Strait/northernmost Baffin Bay dinocyst assemblages suggest cold, icy conditions until ~9 ka BP, followed by a period of relative warmth punctuated by minimum sea ice extent ~6.5 ka BP, and cooling sea surface temperatures and intensifying sea ice cover after ~3.5 ka BP (de Vernal et al., 2013; Levac et al., 2001). In the channels of the northeastern Canadian Arctic, some studies have similarly found evidence for higher temperatures than today and reduced sea ice between 10 and 9 ka BP and 6.5 to 5.5 ka BP and maximum sea ice cover in the last 3–4 kyr (Ledu et al., 2010; Pieńkowski et al., 2012; Vare et al., 2009), although records from the channels are not all in agreement (de Vernal et al., 2013; Ledu et al., 2010). Overall, the similar timing of onset of warmth at sea and on land in this region – including at sites like Deltasø and Wax Lips Lake not located on the outer coast – argues that atmospheric warming did not significantly lag the incursion of warm ocean waters into Baffin Bay (Funder and Weidick, 1991).

Early Holocene warmth recorded by numerous, diverse paleoclimate indicators in this region contrasts with prior observations and climate model simulations indicating that the onset of HTM warmth across the northwest North Atlantic or the Arctic more broadly was delayed by the effects of the residual Laurentide and Fennoscandian ice sheets (Buizert et al., 2018; Kaplan and Wolfe, 2006; Marsicek et al., 2018; Renssen et al., 2009; Zhang et al., 2016, 2017). Many models, for example, suggest temperatures over Greenland did not exceed those of present day until 8 ka BP or after (e.g., Zhang et al., 2017). In contrast, in addition to results from northwest Greenland summarized here, evidence suggests that warmest conditions also occurred in the early Holocene in central east Greenland near Renland Ice Cap (Axford et al., 2017; Vinther et al., 2009). It appears that the Mid to High Arctic sectors of Greenland and the northern Baffin Bay region experienced peak Holocene temperatures during peak summer insolation in the early Holocene when the Laurentide Ice Sheet was still quite large. We also note that early Holocene warmth in this region is registered by both summer and annual proxies, although the majority are probably summer-biased.

4.3. Quantifying Holocene temperature changes

Summer temperatures modeled from chironomids at Deltasø during the HTM were ~2.5–3 °C warmer than modern (surface sediments) and *at least* 3.5–4 °C warmer than the coldest part of the late Holocene. As discussed above in sections 2.4 and 3.2, these estimates for Deltasø are best viewed as minimum constraints on HTM temperature anomalies, and indeed they are near the low end of the range of quantitative estimates from the region (except for the pollen study of Gajewski (2015), which reconstructs later and weaker warmth). Peak HTM summer temperatures 4–7 °C warmer than modern were inferred at nearby Wax Lips Lake (McFarlin et al., 2018). Warm-season temperatures inferred from oxygen isotopes of precipitation at Secret Lake were ~3 °C (2.5–4 °C depending on the model used) warmer than modern and ~4.5 °C warmer than the pre-industrial last millennium between ~7.5 and 6.3 ka (Lasher et al., 2017), but because that record begins at 7.5 ka it provides a *minimum* constraint on peak Holocene warmth. Given local marine limits at ~50 m (Lecavalier et al., 2014), accounting for isostatically depressed elevations during the early Holocene would require adjusting these HTM anomalies downward by a fraction of a degree.

A recent reinterpretation of oxygen isotopes at Agassiz ice cap indicates very warm early Holocene conditions on Ellesmere Island, and a larger magnitude multi-millennial Holocene temperature trend than has been inferred from any other ice core record from Greenland or the Canadian Arctic. Annually integrated temperatures inferred from oxygen isotopes of Agassiz ice cores using the revised elevation corrections were 2.5 °C warmer than modern during the warmest millennium of the HTM (with peak temperatures occurring ~11-10 ka there) and almost 6 °C warmer than the pre-industrial last millennium (Lecavalier et al., 2017, Fig. 7). Inferences from melt layers at Agassiz ice cap indicate that summer temperatures during the ~11-10 ka peak of the HTM were 2–2.5 °C warmer than modern and a (loosely constraining) *minimum* of 3.5–4 °C warmer than the coldest millennium of the late Holocene. Zekollari et al. (2017) argued that geologic data and ice cap modeling from Hans Tausen Ice Cap in Peary Land (~850 km northeast of Deltasø) support extrapolating that large amplitude of warming over a broader region of northern Greenland. Paleotemperature reconstructions from three northwest Greenland lakes (Deltasø, Secret Lake and Wax Lips Lake) now further support Lecavalier et al.'s (2017) reinterpretation of data from Agassiz ice cap.

5. Conclusions and implications

Proxy records from around northwest Greenland including Deltasø provide diverse evidence for strong ocean and atmospheric warming early in the Holocene, with the warmest summer temperatures occurring over land and at sea beginning as early as 11-10 ka BP. Chironomids from Deltasø indicate that peak temperatures during the early Holocene were at least 2.5–3 °C warmer than modern (i.e. than the late 20th and early 21st centuries) and at least 4 °C warmer than the pre-industrial last millennium. Collectively, available quantitative reconstructions suggest ~4–7 °C summer cooling from the early to (pre-industrial) late Holocene over northwest Greenland, with widespread progressive cooling after ~6 ka BP and lowest temperatures in the last millennium. We infer from Deltasø sediments that North Ice Cap was smaller than present throughout most of the Holocene following regional deglaciation ~10.8-10.1 ka BP. The ice cap grew to an extent that dammed Gletschersø and thus meltwater flowed into Deltasø beginning ~1850 AD. Other studies in the Nunatarsuaq region have documented corresponding changes in the nearby Greenland Ice Sheet (Farnsworth et al., 2018; Mörner and Funder, 1990), and Petermann and Humboldt glaciers further north also reached maximum or near-maximum late Holocene positions in the last millennium (Reusche et al., 2018).

Reconstructions of summer air temperatures along Greenland's margins are important for understanding ice sheet sensitivity to temperature change, given that marginal summer temperatures drove past surface melt. The shortage of such data has been a major limitation for validating ice sheet models via comparisons with the geologic record (Lecavalier et al., 2014; Simpson et al., 2009; Sinclair et al., 2016; Young and Briner, 2015). Recent paleotemperature reconstructions from northwest Greenland and the surrounding region, summarized here and by McFarlin et al. (2018), may have important implications for understanding the ice sheet's history. For example, driving an ice sheet model with the high HTM temperatures over northern Greenland inferred from reinterpretation of the Agassiz ice core added almost 1.4 m of sea-level equivalent to the Greenland Ice Sheet's modeled contribution to deglacial sea level rise, a 25% increase in ice sheet mass loss relative to previous simulations assuming moderate HTM warmth (Lecavalier et al., 2017). And as demonstrated by Lecavalier et al. (2014, 2017), a large amplitude of HTM warming in this region would help to resolve model-data discrepancies between modeled Holocene ice sheet changes in northwest Greenland and both relative sea-level data and ice sheet thinning inferred from the Camp Century ice core. Buizert et al. (2018) showed that seasonality of Holocene temperature trends had important consequences for the ice sheet, and that summer temperatures are especially important inputs to ice sheet models. Model-data comparisons elsewhere in Greenland and during other time periods could similarly benefit from development of new local constraints on past ice-marginal summer temperatures (e.g., McFarlin et al., 2018; Sinclair et al., 2016).

Echoing previous work in central east Greenland and on Baffin Island west of Greenland (Axford et al., 2009; Axford et al., 2017; Pendleton et al. in revision), the early warmth documented in northwest Greenland (in both summer and annually integrated proxies) contradicts models that simulate long-delayed onset of warmer-than-present conditions across Greenland due to ongoing climatic effects of the residual Laurentide Ice Sheet (Renssen et al., 2004; Zhang et al., 2016, 2017). Although pulses of Laurentide meltwater may have driven short-term cold reversals in Greenland and surrounding seas repeatedly within the early Holocene (e.g., Jennings et al., 2015), consistent depression of temperatures in northwest and east Greenland for millennia is not evident. Intense early Holocene warmth over northern Greenland could, however, be consistent with Laurentide Ice Sheet effects being manifest primarily within or immediately adjacent to the Labrador Sea (Briner et al., 2016; Kaufman, 2004). This would suggest that many models overestimate the spatial extent of the former ice sheet's effect on climate. Further defining such model-data differences is essential to assessing model performance and understanding mechanisms of past and future climate change.

Acknowledgments

We thank the people and Government of Greenland for granting access to the study site and permission to collect samples (expedition permit #C-12-17 and minerals export permit #094/2012). This work was funded by US NSF PLR-1108306 and PLR-1454734 to YA and PLR-1107411 to EO and MK, research support to YA from the Institute for Sustainability and Energy at Northwestern, a Geological Society of America graduate student grant to GEL, a Weinberg College Undergraduate Research Grant to AP, and Winebaum Fund for Sustainability and Environmental Initiatives undergraduate research support to ET. M. Bigl, L. Corbett and J. Thompson helped

with field work. Thule Air Base, Air Greenland, the U.S. Air Force, the U.S. Air National Guard 109th Airlift Wing, J. Hurley, K. Cosper and Polar Field Services provided logistical support in Greenland. L. Corbett and L. Farnsworth isolated materials for radiocarbon dating and measured loss on ignition at Dartmouth. C. Piske and L. Farnsworth prepared samples for ^{210}Pb dating. D. Johnson measured biogenic silica and C. Carrio and J. McFarlin assisted with chironomid identifications at Northwestern. We thank C. Fortin, A.S. Medeiros and collaborators for making their training set data publically available via the Canadian Cryospheric Information Network's Polar Data Catalogue. LacCore, the University of Minnesota at Duluth Large Lakes Observatory ITRAX XRF core scanning facility and WHOI-NOSAMS provided analytical support. G.A. Milne provided helpful discussion of local elevation history, and two anonymous reviewers provided crucial feedback on this manuscript. Data from this study are publically available from the NOAA National Centers for Environmental Information paleoclimate database/World Data Service for paleoclimatology.

References

Anderson, N.J., Brodersen, K.P., Ryves, D.B., McGowan, S., Johansson, L.S., Jeppesen, E., Leng, M.J., 2008. Climate versus in-lake processes as controls on the development of community structure in a low-arctic lake (South-West Greenland). Ecosystems 11, 307–324.

Antoniades, D., Francus, P., Pienitz, R., St-Onge, G., Vincent, W.F., 2011. Holocene dynamics of the Arctic's largest ice shelf. Proc. Natl. Acad. Sci. U. S. A. 108, 18899–18904.

Appleby, P., Oldfield, F., 1978. The calculation of lead-210 dates assuming a constant rate of supply of unsupported 210Pb to the sediment. Catena 5, 1–8.

Axford, Y., Briner, J.P., Miller, G.H., Francis, D.R., 2009. Paleoecological evidence for abrupt cold reversals during peak Holocene warmth on Baffin Island, Arctic Canada. Quat. Res. 71, 142–149.

Axford, Y., Levy, L.B., Kelly, M.A., Francis, D.R., Hall, B.L., Langdon, P.G., Lowell, T.V., 2017. Timing and magnitude of early to middle Holocene warming in East Greenland inferred from chironomids. Boreas.

Axford, Y., Losee, S., Briner, J.P., Francis, D.R., Langdon, P.G., Walker, I.R., 2013. Holocene temperature history at the western Greenland Ice Sheet margin reconstructed from lake sediments. Quat. Sci. Rev. 59, 87–100.

Bennike, O., 2002. Late quaternary history of Washington land, north Greenland. Boreas 31, 260–272.

Bennike, O., 2004. Holocene sea-ice variations in Greenland: onshore evidence. Holocene 14, 607–613.

Bennike, O., Goodsite, M., Heinemeier, J., 2008. Palaeoecology of Holocene peat deposits from Nordvestø, north-west Greenland. J. Paleolimnol. 40, 557–565.

Berger, A., Loutre, M.-F., 1991. Insolation values for the climate of the last 10 million years. Quat. Sci. Rev. 10, 297–317.

Binford, M.W., 1990. Calculation and uncertainty analysis of 210 Pb dates for PIRLA project lake sediment cores. J. Paleolimnol. 3, 253–267.

Blaauw, M., Christen, J.A., 2018. Rbacon: Age-Depth Modelling Using Bayesian Statistics. R package, version 2.3.4.

Briner, J.P., Håkansson, L., Bennike, O., 2013. The deglaciation and neoglaciation of Upernavik Isstrøm, Greenland. Quat. Res. 80, 459–467.

Briner, J.P., McKay, N.P., Axford, Y., Bennike, O., Bradley, R.S., de Vernal, A., Fisher, D., Francus, P., Fréchette, B., Gajewski, K., Jennings, A., Kaufman, D.S., Miller, G., Rouston, C., Wagner, B., 2016. Holocene climate change in Arctic Canada and Greenland. Quat. Sci. Rev. 147, 340–364.

Briner, J.P., Stewart, H.A.M., Young, N.E., Philipps, W., Losee, S., 2010. Using proglacial-threshold lakes to constrain fluctuations of the Jakobshavn Isbræ ice margin, western Greenland, during the Holocene. Quat. Sci. Rev. 29, 3861–3874.

Brodersen, K.P., Bennike, O., 2003. Interglacial Chironomidae (Diptera) from Thule, Northwest Greenland: matching modern analogues to fossil assemblages. Boreas 32, 560–565.

Brooks, S.J., Axford, Y., Heiri, O., Langdon, P.G., Larocque-Tobler, I., 2012. Chironomids can be reliable proxies for Holocene temperatures. A comment on Velle et al. (2010). Holocene 22, 1495–1500.

Brooks, S.J., Langdon, P.G., Heiri, O., 2007. The identification and use of Palaearctic Chironomidae larvae in palaeoecology. Quat. Res. Assoc.

Buizert, C., Keisling, B.A., Box, J.E., He, F., Carlson, A.E., Sinclair, G., DeConto, R.M., 2018. Greenland-wide seasonal temperatures during the last deglaciation. Geophys. Res. Lett. 45, 1905–1914.

Corbett, L.B., Bierman, P.R., Lasher, G.E., Rood, D.H., 2015. Landscape chronology and glacial history in Thule, northwest Greenland. Quat. Sci. Rev. 109, 57–67.

Davies, S.J., Lamb, H.F., Roberts, S.J., 2015. Micro-Xrf Core Scanning in Palaeolimnology: Recent Developments, Micro-XRF Studies of Sediment Cores. Springer, pp. 189–226.

Dawes, P., 1991. Geological Map of Greenland, 1: 500 000, Thule, Sheet 5. Geological Survey of Greenland, Copenhagen.

Dawes, P.R., 2006. Explanatory Notes to the Geological Map of Greenland, 1: 500 000. Thule, Sheet, p. 5.

Dean Jr., W.E., 1974. Determination of carbonate and organic matter in calcareous sediments and sedimentary rocks by loss on ignition: comparison with other methods. J. Sediment. Petrol. 44, 242–248.

de Vernal, A., Hillaire-Marcel, C., Rochon, A., Fréchette, B., Henry, M., Solignac, S., Bonnet, S., 2013. Dinocyst-based reconstructions of sea ice cover concentration during the Holocene in the Arctic Ocean, the northern North Atlantic Ocean and its adjacent seas. Quat. Sci. Rev. 79, 111–121.

Dyke, A.S., Hooper, J., Savelle, J., 1996. A history of sea ice in the Canadian Arctic archipelago based on postglacial remains of the bowhead whale (Balaena mysticetus). Arctic 49, 235–255.

Eggermont, H., Heiri, O., 2012. The chironomid-temperature relationship: expression in nature and palaeoenvironmental implications. Biol. Rev. Camb. Philos. Soc. 87, 430–456.

Farnsworth, L.B., Kelly, M.A., Bromley, G.R.M., Axford, Y., Osterberg, E.C., Howley, J.A., Jackson, M.S., Zimmerman, S.R., 2018. Holocene history of the Greenland ice-sheet margin in northern Nunatarssuaq, northwest Greenland. Arktos 4.

Fortin, M.-C., Medeiros, A.S., Gajewski, K., Barley, E.M., Larocque-Tobler, I., Porinchu, D.F., Wilson, S.E., 2015. Chironomid-environment relations in northern North America. J. Paleolimnol. 54, 223–237.

Francis, D.R., Wolfe, A.P., Walker, I.R., Miller, G.H., 2006. Interglacial and Holocene temperature reconstructions based on midge remains in sediments of two lakes from Baffin Island, Nunavut, Arctic Canada. Palaeogeogr. Palaeoclimatol. Palaeoecol. 236, 107–124.

Fredskild, B., 1985. The Holocene Vegetational Development of Tugtuligssuaq and Qeqertat, Northwest Greenland. Meddelelser om Grønland, p. 22.

Funder, S., 1978. Holocene stratigraphy and vegetation history in the Scoresby Sund area, East Greenland. Bull. - Gronl. Geol. Undersogelse 1–76.

Funder, S., Goosse, H., Jepsen, H., Kaas, E., Kjær, K.H., Korsgaard, N.J., Larsen, N.K., Linderson, H., Lysa, A., Moller, P., Olsen, J., Willerslev, E., 2011a. A 10,000-year record of Arctic Ocean sea-ice variability–view from the beach. Science 333, 747–750.

Funder, S., Kjeldsen, K.K., Kjær, K.H., Ó Cofaigh, C., 2011b. The Greenland Ice Sheet during the past 300,000 years: a review. In: Ehlers, J., Gibbard, P.L., Hughes, P.D. (Eds.), Quaternary Glaciations - Extent and Chronology. Elsevier, Amsterdam, The Netherlands, pp. 699–713.

Funder, S., Weidick, A., 1991. Holocene boreal molluscs in Greenland—palaeoceanographic implications. Palaeogeogr. Palaeoclimatol. Palaeoecol. 85, 123–135.

Gajewski, K., 2015. Quantitative reconstruction of Holocene temperatures across the Canadian arctic and Greenland. Glob. Planet. Chang. 128, 14–23.

Goldthwait, R., 1960. Study of Ice Cliff in Nunatarssuaq, Greenland, U.S. Army Snow, Ice and Permafrost Research Establishment Technical Report 39. Wilmette, Illinois, p. 106.

Heggen, M.P., Birks, H.H., Anderson, N.J., 2010. Long-term ecosystem dynamics of a small lake and its catchment in west Greenland. Holocene 20, 1207–1222.

Heiri, O., Lotter, A.F., Lemcke, G., 2001. Loss on ignition as a method for estimating organic and carbonate content in sediments: reproducibility and compatibility of result. J. Paleolimnol. 25, 101–110.

Huffman, E.W.D., 1977. Performance of a new automatic carbon-dioxide coulometer. Microchem. J. 22, 567–573.

Jennings, A., Andrews, J., Pearce, C., Wilson, L., Ólfasdótttir, S., 2015. Detrital carbonate peaks on the Labrador shelf, a 13–7ka template for freshwater forcing from the Hudson Strait outlet of the Laurentide Ice Sheet into the subpolar gyre. Quat. Sci. Rev. 107, 62–80.

Jennings, A.E., Sheldon, C., Cronin, T., Francus, P., Stoner, J., Andrews, J., 2011. The Holocene history of Nares Strait. Oceanography 24, 26–41.

Juggins, S., 2007. C2: Software for Ecological and Palaeoecological Data Analysis and Visualisation (User Guide Version 1.5). Newcastle University, Newcastle upon Tyne, p. 77.

Juggins, S., 2013. Quantitative reconstructions in palaeolimnology: new paradigm or sick science? Quat. Sci. Rev. 64, 20–32.

Juggins, S., Birks, H.J.B., 2012. Quantitative Environmental Reconstructions from Biological Data, Tracking Environmental Change Using Lake Sediments, ume 5. Data Handling and Numerical Techniques. Springer, pp. 431–494.

Kaplan, M.R., Wolfe, A.P., 2006. Spatial and temporal variability of Holocene temperature in the North Atlantic region. Quat. Res. 65, 223–231.

Kaufman, D., 2004. Holocene thermal maximum in the western Arctic (0–180°W). Quat. Sci. Rev. 23, 529–560.

Kaufman, D.S., Axford, Y., Anderson, R.S., Lamoureux, S.F., Schindler, D.E., Walker, I.R., Werner, A., 2012. A multi-proxy record of the Last Glacial Maximum and last 14,500 years of paleoenvironmental change at Lone Spruce Pond, southwestern Alaska. J. Paleolimnol. 48, 9–26.

Kaufman, D.S., Axford, Y.L., Henderson, A.C.G., McKay, N.P., Oswald, W.W., Saenger, C., Anderson, R.S., Bailey, H.L., Clegg, B., Gajewski, K., Hu, F.S., Jones, M.C., Massa, C., Routson, C.C., Werner, A., Wooller, M.J., Yu, Z., 2016. Holocene climate changes in eastern Beringia (NW North America) – a systematic review of multi-proxy evidence. Quat. Sci. Rev. 147, 312–339.

Landis, J.D., Renshaw, C.E., Kaste, J.M., 2012. Measurement of 7Be in soils and sediments by gamma spectroscopy. Chem. Geol. 291, 175–185.

Larsen, N.K., Kjær, K.H., Lecavalier, B., Bjørk, A.A., Colding, S., Huybrechts, P., Jakobsen, K.E., Kjeldsen, K.K., Knudsen, K.L., Odgaard, B.V., Olsen, J., 2015. The response of the southern Greenland ice sheet to the Holocene thermal maximum. Geology 43, 291–294.

Larsen, N.K., Levy, L.B., Strunk, A., Søndergaard, A.S., Olsen, J., Lauridsen, T.L., 2019. Local ice caps in finderup land, north Greenland, survived the Holocene thermal maximum. Boreas. https://doi.org/10.1111/bor.12384.
Larsen, N.K., Strunk, A., Levy, L.B., Olsen, J., Bjørk, A., Lauridsen, T.L., Jeppesen, E., Davidson, T.A., 2017. Strong altitudinal control on the response of local glaciers to Holocene climate change in southwest Greenland. Quat. Sci. Rev. 168, 69–78.
Lasher, G.E., Axford, Y., McFarlin, J.M., Kelly, M.A., Osterberg, E.C., Berkelhammer, M.B., 2017. Holocene temperatures and isotopes of precipitation in Northwest Greenland recorded in lacustrine organic materials. Quat. Sci. Rev. 170, 45–55.
Lecavalier, B.S., Fisher, D.A., Milne, G.A., Vinther, B.M., Tarasov, L., Huybrechts, P., Lacelle, D., Main, B., Zheng, J., Bourgeois, J., Dyke, A.S., 2017. High Arctic Holocene temperature record from the Agassiz ice cap and Greenland ice sheet evolution. Proc. Natl. Acad. Sci. U. S. A. 114, 5952–5957.
Lecavalier, B.S., Milne, G.A., Simpson, M.J.R., Wake, L., Huybrechts, P., Tarasov, L., Kjeldsen, K.K., Funder, S., Long, A.J., Woodroffe, S., Dyke, A.S., Larsen, N.K., 2014. A model of Greenland ice sheet deglaciation constrained by observations of relative sea level and ice extent. Quat. Sci. Rev. 102, 54–84.
Ledu, D., Rochon, A., de Vernal, A., St-Onge, G., 2010. Holocene paleoceanography of the northwest passage, Canadian Arctic Archipelago. Quat. Sci. Rev. 29, 3468–3488.
Levac, E., Vernal, A.D., Blake Jr., W., 2001. Sea-surface conditions in northernmost Baffin Bay during the Holocene: palynological evidence. J. Quat. Sci. 16, 353–363.
Levy, L.B., Kelly, M.A., Lowell, T.V., Hall, B.L., Hempel, L.A., Honsaker, W.M., Lusas, A.R., Howley, J.A., Axford, Y.L., 2014. Holocene fluctuations of Bregne ice cap, Scoresby Sund, east Greenland: a proxy for climate along the Greenland Ice Sheet margin. Quat. Sci. Rev. 92, 357–368.
Lowell, T.V., Hall, B.L., Kelly, M.A., Bennike, O., Lusas, A.R., Honsaker, W., Smith, C.A., Levy, L.B., Travis, S., Denton, G.H., 2013. Late Holocene expansion of istorvet ice cap, liverpool land, east Greenland. Quat. Sci. Rev. 63, 128–140.
Marsicek, J., Shuman, B.N., Bartlein, P.J., Shafer, S.L., Brewer, S., 2018. Reconciling divergent trends and millennial variations in Holocene temperatures. Nature 554, 92–96.
McFarlin, J.M., Axford, Y., Osburn, M.R., Kelly, M.A., Osterberg, E.C., Farnsworth, L.B., 2018. Pronounced summer warming in northwest Greenland during the Holocene and last interglacial. In: Proc Natl Acad Sci U S A Published Online June 4 2018.
Medeiros, A.S., Gajewski, K., Porinchu, D.F., Vermaire, J.C., Wolfe, B.B., 2015. Detecting the influence of secondary environmental gradients on chironomid-inferred paleotemperature reconstructions in northern North America. Quat. Sci. Rev. 124, 265–274.
Mörner, N., Funder, S.V., 1990. C-14 Dating of Samples Collected during the NORDQUA 86 Expedition, and Notes on the Marine Reservoir Effect, vol. 22. Meddelelser om Grønland, Geoscience, pp. 63–69.
Mortlock, R.A., Froelich, P.N., 1989. A simple method for the rapid determination of biogenic opal in pelagic marine sediments. Deep-Sea Res. 36, 1415–1426.
Osterberg, E.C., Hawley, R.L., Wong, G., Kopec, B., Ferris, D., Howley, J., 2015. Coastal ice core record of recent Northwest Greenland temperature and sea ice concentration. J. Glaciol 61, 1137–1146. https://doi.org/10.3189/2015JoG15J054.
Pedersen, M., Weng, W.L., Keulen, N., Kokfelt, T., 2013. A new seamless digital 1: 500 000 scale geological map of Greenland. Geol. Surv. Den. Greenl 28, 65–68.
Pendleton, S., Miller, G.H., Lifton, N., Young, N.E., In revision. Cryosphere response resolves conflicting evidence for the timing of peak Holocene warmth on Baffin Island, Arctic Canada. Quat. Sci. Rev.
Pieńkowski, A.J., England, J.H., Furze, M.F.A., Marret, F., Eynaud, F., Vilks, G., Maclean, B., Blasco, S., Scourse, J.D., 2012. The deglacial to postglacial marine environments of SE Barrow Strait, Canadian Arctic Archipelago. Boreas 41, 141–179.
Reeh, N., Thomsen, H., Frich, P., Clausen, H., 1990. Stable isotope studies on the ice margins in the Thule area. In: Funder, S.V. (Ed.), Meddelelser Om Grønland, Geoscience, vol. 22, pp. 47–63.
Reimer, P.J., Bard, E., Bayliss, A., Beck, J.W., Blackwell, P.G., Ramsey, C.B., Buck, C.E., Cheng, H., Edwards, R.L., Friedrich, M., 2013. IntCal13 and Marine13 radiocarbon age calibration curves 0–50,000 years cal BP. Radiocarbon 55, 1869–1887.
Renssen, H., Goosse, H., Fichefet, T., Brovkin, V., Driesschaert, E., Wolk, F., 2004. Simulating the Holocene climate evolution at northern high latitudes using a coupled atmosphere-sea ice-ocean-vegetation model. Clim. Dyn. 24, 23–43.
Renssen, H., Seppä, H., Heiri, O., Roche, D.M., Goosse, H., Fichefet, T., 2009. The spatial and temporal complexity of the Holocene thermal maximum. Nat. Geosci. 2, 411–414.
Reusche, M.M., Marcott, S.A., Ceperley, E.G., Barth, A.M., Brook, E.J., Mix, A.C., Caffee, M.W., 2018. Early to Late Holocene surface exposure ages from two marine-terminating outlet glaciers in northwest Greenland. Geophys. Res. Lett. 45, 7028–7039.
Santisteban, J., Mediavilla, R., Lopez-Pamo, E., Dabrio, C.J., Ruiz Zapata, M.B., Garcia, M.J.G., Castano, S., Martinez-Alfaro, P.E., 2004. Loss on ignition: a qualitative or quantitative method for organic matter and carbonate mineral content in sediments? J. Paleolimnol 32, 287–299.
Saulnier-Talbot, É., Pienitz, R., 2010. Postglacial chironomid assemblage succession in northernmost Ungava Peninsula, Canada. J. Quat. Sci. 25, 203–213.
Shala, S., Helmens, K.F., Luoto, T.P., Salonen, J.S., Väliranta, M., Weckström, J., 2017. Comparison of quantitative Holocene temperature reconstructions using multiple proxies from a northern boreal lake. Holocene 27, 1745–1755.
Simpson, M.J.R., Milne, G.A., Huybrechts, P., Long, A.J., 2009. Calibrating a glaciological model of the Greenland ice sheet from the Last Glacial Maximum to present-day using field observations of relative sea level and ice extent. Quat. Sci. Rev. 28, 1631–1657.
Sinclair, G., Carlson, A.E., Mix, A.C., Lecavalier, B.S., Milne, G., Mathias, A., Buizert, C., DeConto, R., 2016. Diachronous retreat of the Greenland ice sheet during the last deglaciation. Quat. Sci. Rev. 145, 243–258.
Stuiver, M., Reimer, P., Reimer, R., 2017. CALIB 7.1 [WWW program]).
Sutherland, R.A., 1998. Loss-on-ignition estimates of organic matter and relationships to organic carbon in fluvial bed sediments. Hydrobiologia 389, 153–167.
Tjallingii, R., Röhl, U., Kölling, M., Bickert, T., 2007. Influence of the water content on X-ray fluorescence core-scanning measurements in soft marine sediments. Geochem. Geophys. Geosyst. 8, Q02004.
Vare, L.L., Massé, G., Gregory, T.R., Smart, C.W., Belt, S.T., 2009. sea ice variations in the central Canadian arctic archipelago during the Holocene. Quat. Sci. Rev. 28, 1354–1366.
Velle, G., Brodersen, K.P., Birks, H.J.B., Willassen, E., 2010. Midges as quantitative temperature indicator species: lessons for palaeoecology. Holocene 20, 989–1002.
Vinther, B.M., Buchardt, S.L., Clausen, H.B., Dahl-Jensen, D., Johnsen, S.J., Fisher, D.A., Koerner, R.M., Raynaud, D., Lipenkov, V., Andersen, K.K., Blunier, T., Rasmussen, S.O., Steffensen, J.P., Svensson, A.M., 2009. Holocene thinning of the Greenland ice sheet. Nature 461, 385–388.
Wagner, B., Heiri, O., Hoyer, D., 2005. Chironomids as proxies for palaeoenvironmental changes in East Greenland: a Holocene record from geographical society Ø. Z. Dtsch. Ges. Geowiss. 156, 543–556.
Walker, I.R., 2001. Midges: Chironomidae and Related Diptera, Tracking Environmental Change Using Lake Sediments, ume 4. Zoological Indicators. Springer, pp. 43–66.
Walker, I.R., Levesque, J., Cwynar, L.C., Lotter, A.F., 1997. An expanded surface-water paleotemperature inference model for use with fossil midges from eastern Canada. J. Paleolimnol. 18, 165–178.
Walker, I.R., Smol, J.P., Engstrom, D.R., Birks, H.J.B., 1991. An assessment of Chironomidae as quantitative indicators of past climatic change. Can. J. Fish. Aquat. Sci. 48, 975–987.
Walker, M.J.C., Berkelhammer, M., Björck, S., Cwynar, L.C., Fisher, D.A., Long, A.J., Lowe, J.J., Newnham, R.M., Rasmussen, S.O., Weiss, H., 2012. Formal subdivision of the Holocene series/epoch: a discussion paper by a working group of INTIMATE (integration of ice-core, marine and terrestrial records) and the subcommission on quaternary stratigraphy (international commission on stratigraphy). J. Quat. Sci. 27, 649–659.
Weidick, A., Bennike, O., 2007. Quaternary Glaciation History and Glaciology of Jakobshavn Isbræ and the Disko Bugt Region, West Greenland: a Review, vol. 14. Geological Survey of Denmark and Greenland Copenhagen Bulletin, Copenhagen.
Wong, G., Osterberg, E.C., Hawley, R., Courville, Z., Ferris, D., Howley, J., 2015. Coast-to-interior gradient in recent Northwest Greenland precipitation trends (1952-2012). Environ. Res. Lett. 10, 114008. https://doi.org/10.1088/1748-9326/10/11/114008.
Wooller, M.J., Francis, D., Fogel, M.L., Miller, G.H., Walker, I.R., Wolfe, A.P., 2004. Quantitative paleotemperature estimates from δ18O of chironomid head capsules preserved in arctic lake sediments. J. Paleolimnol. 31, 267–274.
Young, N.E., Briner, J.P., 2015. Holocene evolution of the western Greenland Ice Sheet: assessing geophysical ice-sheet models with geological reconstructions of ice-margin change. Quat. Sci. Rev. 114, 1–17.
Zekollari, H., Lecavalier, B.S., Huybrechts, P., 2017. Holocene evolution of Hans Tausen Iskappe (Greenland) and implications for the palaeoclimatic evolution of the high Arctic. Quat. Sci. Rev. 168, 182–193.
Zhang, Y., Renssen, H., Seppä, H., 2016. Effects of melting ice sheets and orbital forcing on the early Holocene warming in the extratropical Northern Hemisphere. Clim. Past 12, 1119–1135.
Zhang, Y., Renssen, H., Seppä, H., Valdes, P.J., 2017. Holocene temperature evolution in the Northern Hemisphere high latitudes – model-data comparisons. Quat. Sci. Rev. 173, 101–113.